RESEARCH ARTICLE SUMMARY

PLANETARY SCIENCE

Distribution of phyllosilicates on the surface of Ceres

E. Ammannito,* M. C. DeSanctis, M. Ciarniello, A. Frigeri, F. G. Carrozzo, J.-Ph. Combe, B. L. Ehlmann, S. Marchi, H. Y. McSween, A. Raponi, M. J. Toplis, F. Tosi, J. C. Castillo-Rogez, F. Capaccioni, M. T. Capria, S. Fonte, M. Giardino, R. Jaumann, A. Longobardo, S. P. Joy, G. Magni, T. B. McCord, L. A. McFadden, E. Palomba, C. M. Pieters, C. A. Polanskey, M. D. Rayman, C. A. Raymond, P. M. Schenk, F. Zambon, C. T. Russell

INTRODUCTION: The surface of the dwarf planet Ceres is known to host phyllosilicate minerals, but their distribution and origin have not previously been determined. Phyllosilicates are hydrated silicates, and their presence on the surface of Ceres is intriguing given that their structure evolves through an aqueous alteration process. In addition, some phyllosilicates are known to bear NH_4, which places a constraint on the pH and redox conditions during the evolution of Ceres. We studied the distribution of phyllosilicates across the planet's surface to better understand the evolutionary pathway of Ceres.

RATIONALE: Using the data acquired by the mapping spectrometer (VIR) onboard the Dawn spacecraft, we mapped the spatial distribution of different minerals on Ceres on the basis of their diagnostic absorption features in visible and infrared spectra. We studied the phyllosilicates through their OH-stretch fundamental absorption at about 2.7 μm and through the NH_4 absorption at about 3.1 μm. From our composition maps, we infer the origin of the materials identified.

ON OUR WEBSITE

Read the full article at http://dx.doi.org/10.1126/science.aaf4279

RESULTS: We found that Mg- and NH_4-bearing phyllosilicates are ubiquitous across the surface of Ceres and that their chemical composition is fairly uniform. The widespread presence of these two types of minerals is a strong indication of a global and extensive aqueous alteration—i.e., the presence of water at some point in Ceres' geological history. Although the detected phyllosilicates are compositionally homogeneous, we found variations in the intensity of their absorption features in the 3-μm region of the reflectance spectrum. Such variations are likely due to spatial variability in relative mineral abundance (see the figure).

CONCLUSION: The large-scale regional variations evident in the figure suggest lateral heterogeneity in surficial phyllosilicate abundance on scales of several hundreds of kilometers. Terrains associated with the Kerwan crater (higher concentration of phyllosilicates) appear smooth, whereas the Yalode crater (lower concentration of phyllosilicates) is characterized by both smooth and rugged terrains. These distinct morphologies and phyllosilicate concentrations observed in two craters that are similar in size may reflect different compositions and/or rheological properties. On top of this large-scale lateral heterogeneity, small-scale variations associated with individual craters could result from different proportions of mixed materials in a stratified upper crustal layer that has been exposed by impacts. Variations associated with fresh craters, such as the 34-km-diameter Haulani, indicate the presence of crustal variations over a vertical scale of a few kilometers, whereas much larger craters, such as the 126-km-diameter Dantu, suggest that such stratification may extend for at least several tens of kilometers. ■

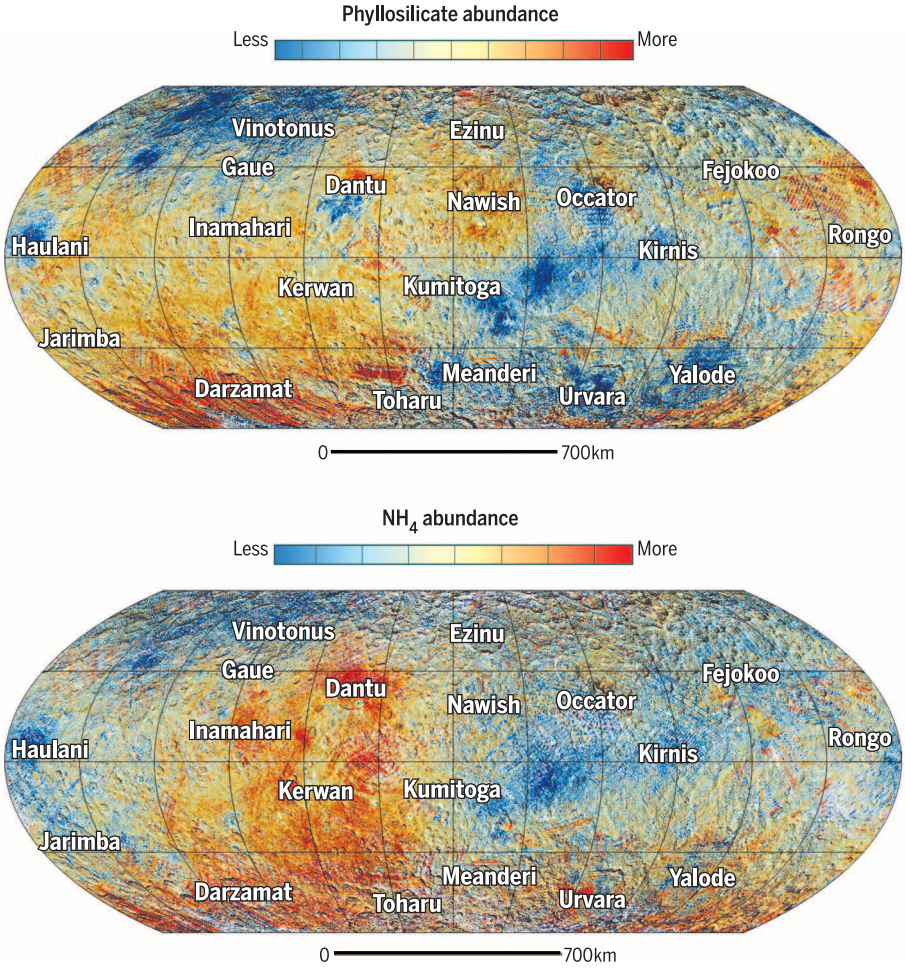

Abundance maps. Qualitative maps of the abundances of (**top**) phyllosilicates and (**bottom**) NH_4, based on the depth of their absorption features. The two maps have a similar global pattern, although they differ in some localized regions such as Urvara. The scale bar is valid at the equator.

The list of author affiliations is available in the full article online.
*Corresponding author. Email: eleonora.ammannito@igpp.ucla.edu
Cite this article as E. Ammannito *et al.*, *Science* **353**, aaf4279 (2016). DOI: 10.1126/science.aaf4279

RESEARCH ARTICLE

PLANETARY SCIENCE

Distribution of phyllosilicates on the surface of Ceres

E. Ammannito,[1]* M. C. DeSanctis,[2] M. Ciarniello,[2] A. Frigeri,[2] F. G. Carrozzo,[2] J.-Ph. Combe,[3] B. L. Ehlmann,[4,5] S. Marchi,[6] H. Y. McSween,[7] A. Raponi,[2] M. J. Toplis,[8] F. Tosi,[2] J. C. Castillo-Rogez,[5] F. Capaccioni,[2] M. T. Capria,[2] S. Fonte,[2] M. Giardino,[2] R. Jaumann,[9] A. Longobardo,[2] S. P. Joy,[1] G. Magni,[2] T. B. McCord,[3] L. A. McFadden,[10] E. Palomba,[2] C. M. Pieters,[11] C. A. Polanskey,[5] M. D. Rayman,[5] C. A. Raymond,[5] P. M. Schenk,[12] F. Zambon,[2] C. T. Russell[1]

The dwarf planet Ceres is known to host phyllosilicate minerals at its surface, but their distribution and origin have not previously been determined. We used the spectrometer onboard the Dawn spacecraft to map their spatial distribution on the basis of diagnostic absorption features in the visible and near-infrared spectral range (0.25 to 5.0 micrometers). We found that magnesium- and ammonium-bearing minerals are ubiquitous across the surface. Variations in the strength of the absorption features are spatially correlated and indicate considerable variability in the relative abundance of the phyllosilicates, although their composition is fairly uniform. These data, along with the distinctive spectral properties of Ceres relative to other asteroids and carbonaceous meteorites, indicate that the phyllosilicates were formed endogenously by a globally widespread and extensive alteration process.

The surface of the dwarf planet Ceres exhibits low reflectance and a relatively featureless spectrum in the range of 0.5 to 2.6 μm, with the exception of a broad absorption feature centered around 1.2 μm (*1*,*2*). Thermally corrected reflectance data from 2.6 to 4.2 μm, measured from onboard the Dawn spacecraft, reveal a spectrum rich in absorption features at 2.72, 3.05 to 3.1, 3.3 to 3.5, and 3.95 μm, which are diagnostic of the composition of the surface (*3*). The band from 3.05 to 3.1 μm is clearly visible in ground-based spectra and has been attributed to a variety of different phases including water ice (*4*), hydrated or NH_4-bearing clay minerals (*5*, *6*), or brucite (*7*), whereas the 3.95-μm band has been definitively attributed to carbonates (*8*). Initial Dawn observations obtained during the Approach and Survey phases of the mission indicate that Ceres' average surface is a mixture of NH_4-bearing phyllosilicates such as serpentines and smectites, carbonates, and absorbing dark materials such as organic carbon or magnetite (*3*). As Dawn has continued to orbit Ceres (*9*), the visible and infrared mapping spectrometer onboard the spacecraft [VIR (*10*)] has obtained spatially resolved hyperspectral images of Ceres, which have been projected to generate maps of spectral parameters that characterize Ceres' mineralogy. Dawn's orbital characteristics and the orientation of Ceres' spin axis (*11*) have enabled 84% of the surface to be mapped with the VIR's infrared channel. The maps discussed here have roughly 1.1-km spatial resolution, global longitude coverage, and latitude coverage spanning from 60°S to 60°N (see the Materials and methods section for further details). All the maps and coordinates are given using the Kait Prime Meridian Reference System (*12*).

Albedo at 0.55 μm, measured by the VIR

The geometric albedo measured by the VIR instrument is 0.094 ± 0.008 at 0.55 μm (Materials and methods section). Given the low albedo of the surface, single scattering dominates the surface reflectance. Figure 1 is an albedo map, in reflectance at standard geometry, indicating a variable proportion of low- and high-albedo materials on Ceres' surface. Roughly 70% of the mapped surface has a radiance factor (I/F, defined as π × reflectance, where I is the measured radiance and F is solar flux) at 0.55 μm that is within the range 0.032 to 0.036, with a central value of 0.034.

Shown in Fig. 2A is an example of a typical thermally corrected reflectance spectrum of Ceres acquired by VIR. Diagnostic absorptions at 2.7 and 3.05 to 3.1 μm are well defined, and we measured and mapped the strength of these features globally across Ceres (Fig. 3 and Materials and methods section).

Variability of the 2.7- and 3.1-μm absorption bands

The strong and narrow absorption near 2.7 μm is an OH-stretch fundamental, centered at 2.72 to 2.73 μm (*13*). This relatively strong absorption dominates the overall spectral properties and is a distinctive indicator of OH-bearing minerals such as phyllosilicates (*14*). The exact spectral position of the absorption is indicative of Mg-OH phases, such as antigorite (Mg-serpentine) or saponite (Mg-smectite) (*15*). We found that the spectral

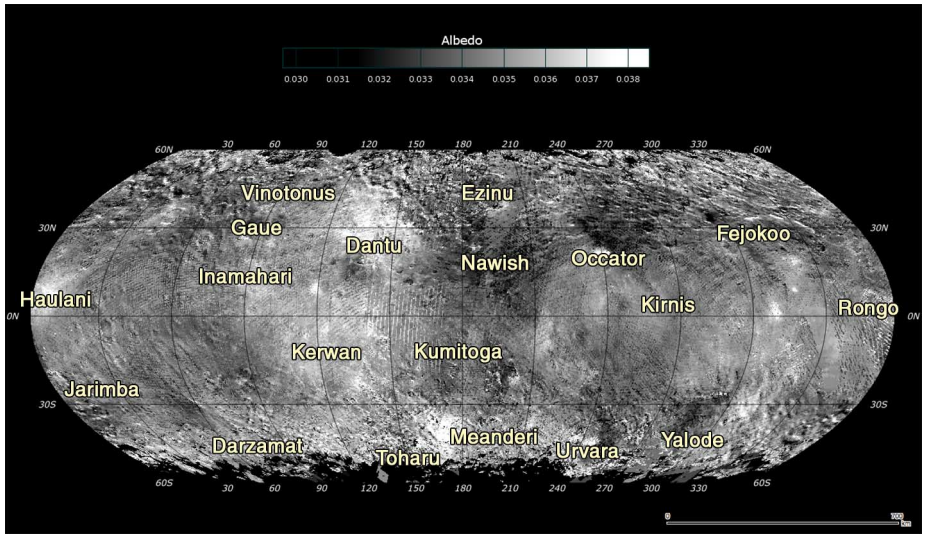

Fig. 1. Albedo map. The map shows the albedo in terms of the radiance factor (I/F) at 0.55 μm, photometrically corrected and converted to standard observation geometry (incidence angle = 30°, emission angle = 0°, phase angle = 30°). Some of the brightest regions are out of scale, namely, Occator, Toharu, and Haulani. The scale bar is true at the equator.

[1]Earth Planetary and Space Sciences, University of California–Los Angeles, 603 Charles Young Drive, Los Angeles, CA 90095-1567, USA. [2]Istituto di Astrofisica e Planetologia Spaziali, Istituto Nazionale di Astrofisica, 00133 Roma, Italy. [3]The Bear Fight Institute, Winthrop, WA 98862, USA. [4]Division of Geological and Planetary Sciences, California Institute of Technology, Pasadena, CA 91125, USA [5]Jet Propulsion Laboratory, California Institute of Technology, Pasadena, CA 91109, USA. [6]Southwest Research Institute, Boulder, CO 80302, USA. [7]Department of Earth and Planetary Sciences, University of Tennessee, Knoxville, TN 37996-1410, USA. [8]Institut de Recherche en Astrophysique et Planétologie (UMR 5277), Université de Toulouse, F-31400 Toulouse, France. [9]Institute of Planetary Research, Deutsches Zentrum für Luft- und Raumfahrt, 12489 Berlin, Germany. [10]NASA Goddard Space Flight Center, Greenbelt, MD 20771, USA. [11]Department of Earth, Environmental, and Planetary Sciences, Brown University, Providence, RI 02912, USA. [12]Lunar and Planetary Institute, Houston, TX 77058, USA.
*Corresponding author. Email: eleonora.ammannito@igpp.ucla.edu

position of this absorption does not vary significantly across the mapped portion of the surface (2.727 ± 0.003 μm; Materials and methods section), which is an indication that the chemical composition of the phyllosilicates does not change substantially. Within the mapped portion of Ceres, the only locations that shift toward longer wavelengths, and therefore that point to a different chemical composition of the phyllosilicates, are the small bright regions on the floor of Occator crater (*16*). Mg-rich serpentines are commonly present in carbonaceous chondrite meteorites, along with a large number of other distinct phyllosilicates (*14*). Carbonaceous chondrites in the CM group have matrix compositions that systematically vary from the least aqueously altered samples, which have a 2.7-μm absorption consistent with cronstedtite (Fe-serpentine), to the most aqueously altered samples, which have shorter wavelength absorptions characteristic of antigorite (Mg-serpentine) (*17*). The pervasive presence of Mg- rather than Fe-serpentine across Ceres thus indicates that aqueous alteration has been extensive. Although the presence and the position of the 2.7-μm absorption are globally constant, its intensity shows significant variations beyond the 2σ errors associated with the measurements. The computed average value is 0.251 ± 0.006, and the range of variability is between 0.226 and 0.270. The spatial distribution of the 2.7-μm band depth (Fig. 3A) shows two broad regions containing terrains in which the values of the band depths are lower than the average (blue in Fig. 3A). One region is in the northeast quadrant and the other is in the southwest. In contrast, the region around the smooth Kerwan terrains has deeper Mg-OH band depths with respect to the nearby regions; specific regions near the northern Dantu and northeastern Occator craters also have deeper band depths. The lack of geochemical variation inferred from the band center position suggests either that the exposed upper layer has no substantive phyllosilicate compositional gradient or that some homogenization process has been very efficient at the spatial scale sampled by VIR. The latter is unlikely because although the position of the bands do not vary, there are variations in the intensity of the same absorption in some craters (Haulani, Dantu, and Urvara), and a homogenization process would have affected both parameters.

The distinct absorption feature at about 3.1 μm has been attributed to ammoniated phyllosilicates (*3*, *5*). The analysis of this feature shows that its band center position does not vary across the surface, and its value, computed after removal of the local continuum, is 3.061 μm with a standard deviation of 0.011 μm (Materials and methods section). As with the 2.7-μm absorption, the absence of variability in the central wavelength of the 3.1-μm absorption suggests that the ammoniated phyllosilicate phase is compositionally homogeneous over most of Ceres' surface. The average value of the intensity of the 3.1-μm absorption is 0.055 (with a standard deviation of 0.012). The spatial variability in the 3.1-μm band intensity (Fig. 3B) broadly follows that of the 2.7-μm band (Fig. 3A), with the same broad regions described above. However, at smaller spatial scales, there are locations where intensity variations are inversely correlated (e.g., the Urvara crater), whereas elsewhere the intensities of the two absorption features show a weak positive correlation (Fig. 4A). In contrast, neither the 2.7- nor the 3.1-μm band exhibits an intensity that meaningful correlates at the global scale with the I/F ratio (Fig. 4, B and C), although a correlation is sometimes evident locally, as in the Haulani crater.

The Haulani crater (5.7°N, 10.9°E; diameter, 34 km) and its ejecta stand out in the global maps (Figs. 1, 3A, and 3B), showing high albedo but shallower bands with respect to the surroundings (Fig. 5B). The shallowest bands (blue color in Fig. 5A and blue spectrum in Fig. 5B) are found inside the crater and in nearby bright ejecta. In this crater, the shallow bands are associated with bright material that was excavated and deposited by the impact. However, as noted above, the anticorrelation of band depth and albedo is not global. A second example is the Dantu crater (24.35°N, 138.2°E; diameter, 126 km), which is divided into two terrains: the northern area, with higher band depths (yellow spectrum in Fig. 5, C and D), and the southern area, with shallower bands (blue in Fig. 5, C and D). Unlike in Haulani, in Dantu, there is no correlation between band depth and albedo. The area just outside the northern rim of the crater has a similar albedo to that of the floor, whereas the deepest absorptions are found only within the rim.

Implications of variability in the band intensities

Variations in the band depth could be due to a variety of factors, such as (i) relative abundance and grain size of spectrally opaque dark phases, (ii) phase changes caused by impact processes (e.g., dehydration), (iii) variations in the quantity of impact-delivered material, (iv) depth-dependent variation in the abundances of materials exposed by craters, and/or (v) heterogeneity of the external layer of the surface.

The relative abundance and size of opaque phases in a mixture has a major effect on spectral contrast and the strength of absorption bands, as well as on albedo. With increasing abundance of fine-grained opaque content, albedo and band strength decrease nonlinearly (*18*, *19*). Thus, band strength should be correlated with albedo. Given that this is not observed on Ceres, variation in opaque content cannot account for the observed variations in band strength.

Dehydration of phyllosilicates at increased temperatures generated by impacts should reduce the intensity of the OH-stretch band at 2.7 μm (*20*, *21*) and of the NH_4-related band at 3.1 μm (*20*, *22*). However, prominent craters such as Kerwan (diameter, 280 km) are associated with deeper absorption bands, whereas the similar-sized crater Yalode (diameter, 260 km) is associated with much shallower bands. Although it is conceivable that impact heating could have been

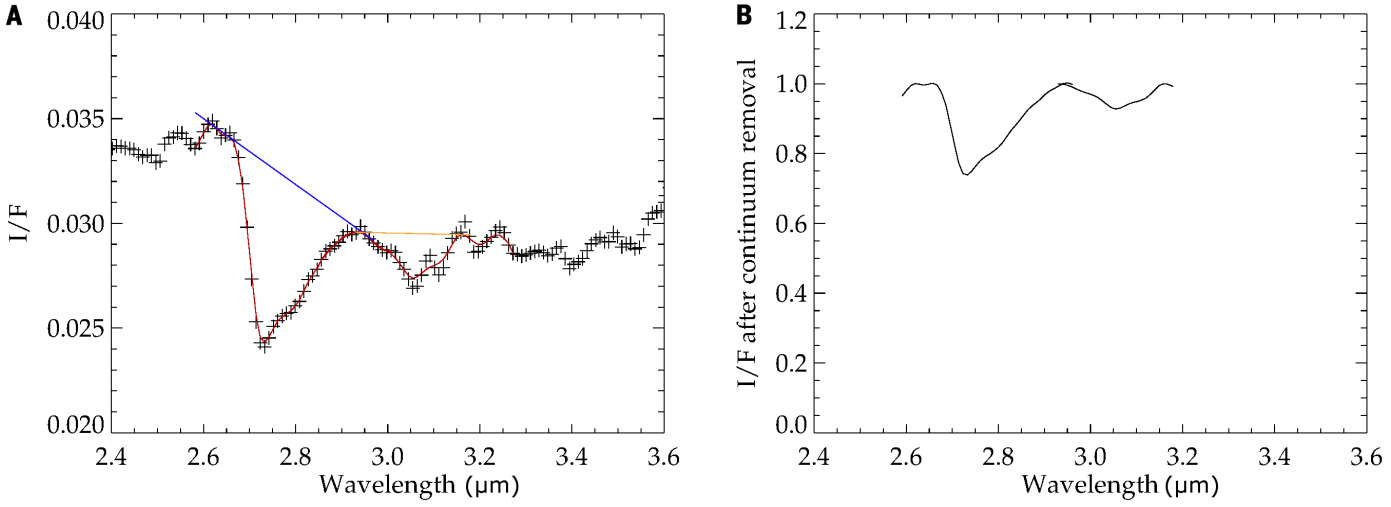

Fig. 2. Computation of band parameters. (**A**) Example Ceres spectrum (black crosses) with the smoothed spectrum superimposed (red line). The blue and yellow lines represent the straight line used to compute the continuum of each band. (**B**) Continuum-removed spectrum (black line).

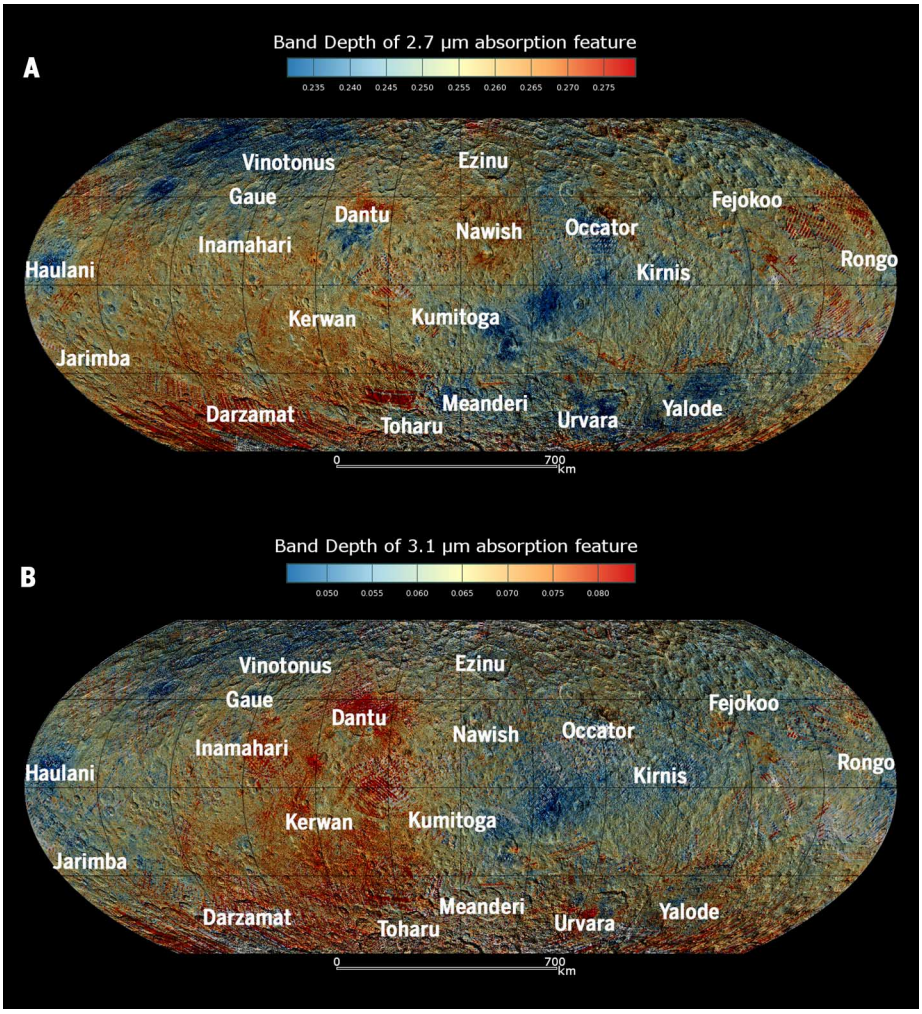

Fig. 3. Band depth maps. Maps of the peak absorption depths of (**A**) the 2.7-μm OH-stretch band and (**B**) the 3.1-μm NH_4 band. The two maps have a similar global pattern, although they differ in some localized regions such as Urvara. The scale bar is true at the equator.

different in these two cratering events, it is unlikely to be the cause of the observed spatial heterogeneity. Furthermore, there are craters, such as Dantu, that expose diverse materials with both deeper and shallower band depths.

The band depth distribution does not correlate with crater size or inferred age. For instance, the pristine morphologies of the Dantu and Haulani craters suggest recent formation [Dantu certainly postdates Kerwan on the basis of superposition (*23*)]. The fact that craters of very different sizes and formation ages show heterogeneities reduces the likelihood that contamination from impactor materials and space weathering is a principal cause of the observed distribution of band depth variations. This conclusion is also reinforced by the constant position of the absorption band centers across the surface, limiting the potential role of contamination from impactor materials (unless they had exactly the same composition as Ceres, which seems unlikely, given the wide range of asteroid spectra and chondrite compositions).

The most likely explanation is that the variability in the strengths of these two diagnostic mineral absorptions is associated with a variation in the abundance of phyllosilicates relative to the other components of the surface. According to the modeling technique used in (*3*), the range of variability observed on Ceres is compatible with abundance variations in the range of 6 to 12% and 3 to 9% for Mg-rich phyllosilicates and NH_4-bearing species, respectively. We stress that the data indicate that the composition of phyllosilicate species is constant, but that it is their relative abundance that varies. Therefore, the correlation expressed in Fig. 4A between the depths of the absorptions at 2.7 and 3.1 μm indicates that the abundances of Mg-phyllosilicates and ammoniated phyllosilicates are generally correlated. In combination with the absence of Fe-phyllosilicates, this suggests that the ammoniated phyllosilicates, as well as the other phyllosilicates, are endogenous, and that the aqueous alteration processes creating such minerals were global and not due to the local environment.

The distribution of measured spectral properties is compatible with the presence on Ceres of a single Mg-phyllosilicate composition, sometimes including embedded ammonium. However, we cannot exclude the possibility of a collection of phyllosilicates defining a spatially homogeneous composition. Current thermal evolution models for Ceres (*24*, *25*) are compatible with an evolutionary pathway that starts from a parent body of primitive carbonaceous chondrite–like material, which undergoes aqueous alteration processes in a hydrothermal environment whose pH and redox conditions favor the stability of ammonium (over ammonia). The substitution of potassium and, to a lesser extent, alkali earth metals by ammonium is a well-understood phenomenon resulting in the production of Mg- and NH_4-bearing clays (e.g., *26* and references therein).

Although the Ceres phyllosilicates are compositionally homogeneous, we interpret the observed variations in the depth of absorptions in the 3-μm region as an indication of variability in their abundance. The large-scale regional variations shown in Fig. 3, A and B, suggest lateral heterogeneity in phyllosilicate abundance over a scale of several hundreds of kilometers. Terrains associated with Kerwan (higher concentration of phyllosilicates) appear smooth in texture, whereas Yalode (lower concentration of phyllosilicates) is characterized by both smooth and rugged terrains (*27*). This pronounced difference in morphology and phyllosilicate concentration between two craters that are similar in size may reflect different compositions and/or rheological properties. On top of this large-scale lateral heterogeneity, we found small-scale variations associated with craters (examples in Fig. 5) that could result from different proportions of mixed materials in a stratified upper layer exposed by impacts. Fresh craters such as Haulani indicate the presence of different materials over a vertical scale of a few kilometers, whereas much larger craters such as Dantu suggest that such stratification may extend for at least several tens of kilometers.

Materials and methods

VIR measurements at Ceres

The Dawn spacecraft has been acquiring data about the dwarf planet Ceres since January 2015 (*11*). During the Approach phase (January to April 2015), there were nine opportunities to point the optical instruments toward Ceres and to acquire spectral information about its surface. In late April/early May 2015, the spacecraft performed an observational campaign while the spacecraft was in orbit around Ceres at an altitude of 13,600 km. In this mission phase, called RC3, the instruments acquired limb and high phase images while the spacecraft was on the night side of the orbit and nadir images while it was on the day side. After this initial part of the exploration, in three consequent orbits Survey (4400-km altitude), High Altitude Mapping Orbit (HAMO, 1470-km altitude) and Low Altitude Mapping Orbit (LAMO, 385-km altitude), the instruments acquired data in the dayside section of the orbit at increasing resolution. The spectrometer VIR (visible channel: 0.25- to 1.0-μm range and 0.002-μm resolution; infrared channel: 1.0- to 5.0-μm range and 0.010-μm resolution) acquired data during all the mapping

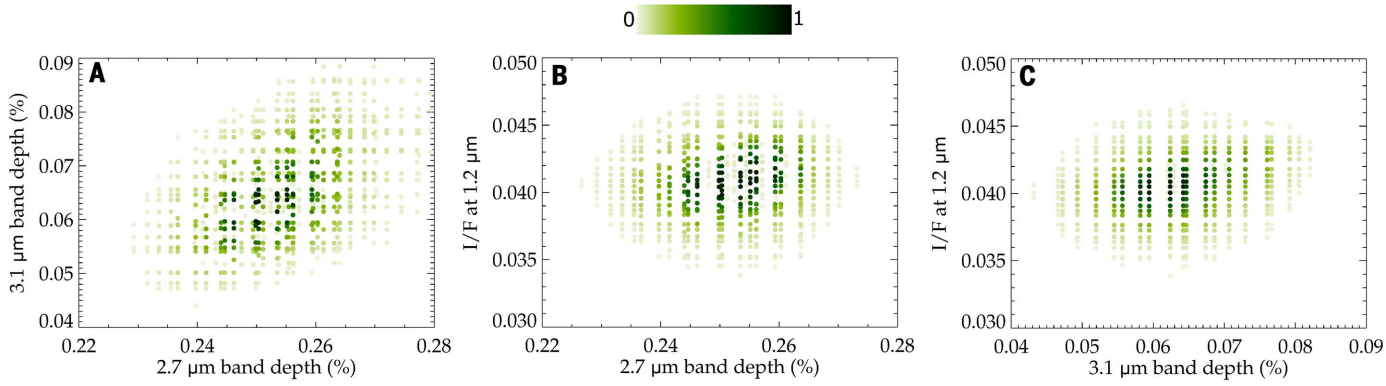

Fig. 4. Scatterplots of Ceres global spectral parameters associated with diagnostic absorptions. (**A**) 3.1-μm band absorption depth versus 2.7-μm band absorption depth. (**B**) *I/F* at 1.2 μm versus 2.7-μm band absorption depth. (**C**) *I/F* at 1.2 μm versus 3.1-μm band absorption depth. The color scale represents the frequency of each data point normalized to the maximum value in each plot.

orbits, although in this paper we used data from RC3 and Survey. In RC3, VIR acquired 1.9 million infrared spectra and 1.9 million visible spectra with an average linear resolution of 3.4 km. In Survey orbit, VIR acquired 2.8 million infrared spectra and 4.3 million visible spectra with an average linear resolution of 1.1 km. Resolutions indicated here do not consider the smearing.

Geometric albedo and albedo maps

Geometric albedo is computed from eq. 12.58 in (*28*)

$$A_p(w,\bar{\theta}) = \frac{w}{8}\{[1+B_0]p(0)-1\} + U(w,\bar{\theta})\frac{r_0}{2}\left(1+\frac{r_0}{3}\right)$$

where w is the single scattering albedo, B_0 is the opposition effect amplitude, $p(0)$ is the single particle phase function at 0° phase angle, and $U(w,\bar{\theta})$ accounts for large scale surface roughness through the slope parameter $\bar{\theta}$. Hapke's model parameters derived in (*29*) from spectrophotometric analysis of VIR observations of Ceres have been assumed.

Albedo map has been produced by reporting VIR measured radiance factor (*I/F*) with generic incidence, emission, and phase angles (i, e, α) to standard observation geometry (i = 30°, e = 0°, α = 30°) by means of the relation

$$I/F(30^\circ,0^\circ,30^\circ) = \frac{I/F(i,e,\alpha)}{I/F_{\mathrm{m}}(i,e,\alpha)} I/F_{\mathrm{m}}(30^\circ,0^\circ,30^\circ)$$

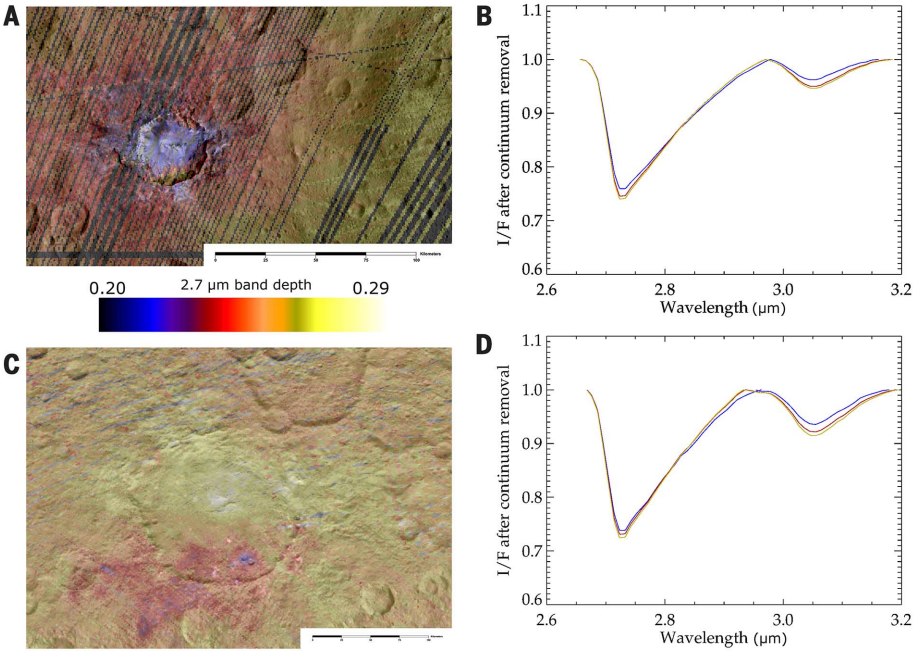

Fig. 5. Haulani and Dantu craters. (**A** and **B**) Haulani. (**C** and **D**) Dantu. For each crater, we show a map of the 2.7-μm band depth [(A) and (C)] and the continuum-removed spectra [(B) and (D)]. Each spectrum shown here is an average of locations in the image that share the same band depth. The color of each spectrum corresponds to the band depth.

where the subscript m indicates that reflectance has been modeled applying Hapke's theory (*28*) as shown in (*29*).

Band parameters

The band parameters have been computed with the following steps: (i) Removal of thermal emission. The thermal emission has been modeled as the Planck function that best fit the measured *I/F*. (ii) Smoothing of the spectra (from black crosses to red line in Fig. 2A). The spectra have been smoothed with a boxcar average of 3 spectral channels. (iii) Evaluation of the continuum and continuum removal. The band continuum of each band has been computed as the straight line between the two local maxima (blue line for 2.7-μm band and orange line for 3.1-μm band in Fig. 2A). The continuum-removed spectrum is the ratio of the smoothed spectrum and the continuum. (iv) Band centers: after the continuum removal, the band center is the wavelength which corresponds to the local minimum after the continuum removal (Fig. 2B). (v) Band depths are defined as $1–R_c/R_b$, where R_b is the reflectance at the band minimum and R_c is the reflectance of the continuum at the same wavelength as R_b.

Photometric correction of band parameters

Band centers have not been corrected. Band depths (*BD*) have been rescaled to a reference condition with emission angle (e) equal to 0°, incidence angle (i) equal to 30°, and phase angle (φ) equal to 30°. The scaling has been done using an empirical approach. According to this approach, the rescaled band depth ($BD_{(0,30,30)}$) can be computed as

$$BD_{(0,30,30)} = BD_{(e,i,\varphi)} \times LS \times f_\lambda(\varphi)$$

where $BD_{(e,i,\varphi)}$ is the band depth computed according to the procedure described in the previous paragraph, *LS* is the Lommel Seeliger factor

$$LS = 0.46 \times \frac{\cos i + \cos e}{\cos i}$$

and $f_\lambda(\varphi)$ is the phase function of each absorption band that has been modeled with a polynomial of the second order

$$f_{2.7}(\varphi) = \frac{0.26}{0.25 - 8.62{*}10^{-5}{*}\varphi + 1.33{*}10^{-5}{*}\varphi^2}$$

$$f_{3.1}(\varphi) = \frac{0.08}{0.07 - 2.60{*}10^{-4}{*}\varphi + 1.12{*}10^{-5}{*}\varphi^2}$$

Maps of band parameters

The RC3 and Survey data sets have been mapped using a Mollweide projection in the latitude range 60°S to 60°N. Data from both mission phases have been filtered for illumination conditions and level of reflectance. In the maps of the band parameters, only the spectra with incidence and emission angles lower than 70°, phase angle between 15° and 60°, and average I/F brightness higher than 0.004 have been considered. To generate the maps discussed in this work, rather than an average, the RC3 map has been used only to fill the gaps in the Survey-based map.

REFERENCES AND NOTES

1. S. J. Bus, R. P. Binzel, Phase II of the small main-belt asteroid spectroscopic survey: The observations. *Icarus* **158**, 106–145 (2002). doi: 10.1006/icar.2002.6857
2. S. J. Bus, R. P. Binzel, Phase II of the small main-belt asteroid spectroscopic survey: A feature-based taxonomy. *Icarus* **158**, 146–177 (2002). doi: 10.1006/icar.2002.6856
3. M. C. De Sanctis *et al*., Ammoniated phyllosilicates with a likely outer Solar System origin on (1) Ceres. *Nature* **528**, 241–244 (2015). doi: 10.1038/nature16172; pmid: 26659184
4. L. A. Lebofsky, M. A. Feierberg, A. T. Tokunaga, H. P. Larson, J. R. Johnson, The 1.7–4.2 μm spectrum of asteroid 1 Ceres: Evidence for structural water in clay minerals. *Icarus* **48**, 453–459 (1981). doi: 10.1016/0019-1035(81)90055-5
5. T. V. King, R. N. Clark, W. M. Calvin, D. M. Sherman, R. H. Brown, Evidence for ammonium-bearing minerals on Ceres. *Science* **255**, 1551–1553 (1992). doi: 10.1126/science.255.5051.1551; pmid: 17820166
6. P. Vernazza *et al*., Analysis of near-IR spectra of 1 Ceres and 4 Vesta, targets of the Dawn mission. *Astron. Astrophys.* **436**, 1113–1121 (2005). doi: 10.1051/0004-6361:20042506
7. R. E. Milliken, A. S. Rivkin, Brucite and carbonate assemblages from altered olivine-rich materials on Ceres. *Nat. Geosci.* **2**, 258–261 (2009). doi: 10.1038/ngeo478
8. A. S. Rivkin, E. L. Volquardsen, B. E. Clark, The surface composition of Ceres: Discovery of carbonates and iron-rich clays. *Icarus* **185**, 563–567 (2006). doi: 10.1016/j.icarus.2006.08.022
9. C. T. Russell, C. A. Raymond, The Dawn Mission to Vesta and Ceres. *Space Sci. Rev.* **163**, 3–23 (2011). doi: 10.1007/s11214-011-9836-2
10. M. C. De Sanctis *et al*., The VIR spectrometer. *Space Sci. Rev.* **163**, 329–369 (2011). doi: 10.1007/s11214-010-9668-5
11. C. T. Russell *et al*., Dawn arrives at Ceres: Exploration of a small volatile-rich world. *Science* **353**, 1008–1010 (2016).
12. T. Roatsch *et al*., Ceres Survey Atlas derived from Dawn Framing Camera images. *Planet. Space Sci.* **121**, 115–120 (2016). doi: 10.1016/j.pss.2015.12.005
13. V. C. Farmer, "The layer silicates," in *The Infrared Spectra of Minerals* (Monograph 4, The Mineralogical Society of Great Britain and Ireland, 1974), pp. 331–363.
14. A. J. Brearley, Phyllosilicates in the matrix of the unique carbonaceous chondrite Lewis Cliff 85332 and possible implications for the aqueous alteration of CI chondrites. *Meteoritics* **32**, 377–388 (1997). doi: 10.1111/j.1945-5100.1997.tb01281.x
15. J. L. Bishop, M. D. Lane, M. D. Dyar, A. J. Brown, Reflectance and emission spectroscopy study of four groups of phyllosilicates: Smectites, kaolinite-serpentines, chlorites and micas. *Clay Miner.* **43**, 35–54 (2008). doi: 10.1180/claymin.2008.043.1.03
16. M. C. De Sanctis *et al*., Bright carbonate deposits as evidence of aqueous alteration on (1) Ceres. *Nature* **536**, 54–57 (2016). doi: 10.1038/nature18290; pmid: 27362221
17. D. Takir *et al*., Nature and degree of aqueous alteration in CM and CI carbonaceous chondrites. *Meteorit. Planet. Sci.* **48**, 1618–1637 (2013).
18. R. N. Clark, Spectral properties of mixtures of montmorillonite and dark carbon grains: Implications for remote sensing minerals containing chemically and physically adsorbed water. *J. Geophys. Res.* **88**, 10635–10644 (1983). doi: 10.1029/JB088iB12p10635
19. C. M. Pieters, Strength of mineral absorption features in the transmitted component of near-infrared reflected light: First results from RELAB. *J. Geophys. Res.* **88**, 9534–9544 (1983). doi: 10.1029/JB088iB11p09534
20. J. D. Russell, V. C. Farmer, Infra-red spectroscopic study of the dehydration of montmorillonite and saponite. *Clay Miner. Bull.* **5**, 443–464 (1964). doi: 10.1180/claymin.1964.005.32.04
21. R. L. Frost, A. M. Vassallo, The dihydroxylation of the kaolinite clay minerals using infrared emission spectroscopy. *Clays Clay Miner.* **44**, 635–651 (1996). doi: 10.1346/CCMN.1996.0440506
22. B. Chourabi, J. J. Fripiat, Determination of tetrahedral substitutions and interlayer surface heterogeneity from vibrational spectra of ammonium in smectites. *Clays Clay Miner.* **29**, 260–268 (1981). doi: 10.1346/CCMN.1981.0290403
23. H. Hiesinger *et al*., Cratering on Ceres: Implications for its crust and evolution. *Science* **353**, aaf4759 (2016).
24. T. B. McCord, C. Sotin, Ceres: Evolution and current state. *J. Geophys. Res.* **110**, E05009 (2005). doi: 10.1029/2004JE002244
25. J. C. Castillo-Rogez, T. B. McCord, Ceres' evolution and present state constrained by shape data. *Icarus* **205**, 443–459 (2010). doi: 10.1016/j.icarus.2009.04.008
26. S. Engel, J. I. Lunine, D. L. Norton, Silicate interactions with ammonia-water fluids on early Titan. *J. Geophys. Res.* **99**, 3745–3752 (1994). doi: 10.1029/93JE03433
27. D. Buczkowski *et al*., The geomorphology of Ceres. *Science* **353**, aaf4332 (2016).
28. B. Hapke, *Theory of Reflectance and Emittance Spectroscopy* (Cambridge Univ. Press, ed. 2, 2012).
29. M. Ciarniello, M. C. De Sanctis, E. Ammannito, A. Raponi, A. Longobardo, E. Palomba, F. G. Carrozzo, F. Tosi, J.-Y. Li, S. Schröder, F. Zambon, A. Frigeri, S. Fonte, M. Giardino, C. M. Pieters, C. A. Raymond, C. T. Russell, http://arxiv.org/abs/1608.04643 (2016).

ACKNOWLEDGMENTS

We thank the Italian Space Agency (ASI), NASA, and the Deutsches Zentrum für Luft- und Raumfahrt for supporting this work. The VIR instrument was funded and coordinated by the ASI and built by Selex ES, with the scientific leadership of the Institute for Space Astrophysics and Planetology, Italian National Institute for Astrophysics, Italy, and it is operated by the Institute for Space Astrophysics and Planetology, Rome, Italy. A portion of this work was carried out at the Jet Propulsion Laboratory, California Institute of Technology, USA, under contract to NASA. Dawn data are archived in NASA's Planetary Data System; VIR spectral data may be obtained at http://sbn.psi.edu/pds/resource/dwncvir.html.

5 February 2016; accepted 29 July 2016
10.1126/science.aaf4279

Distribution of phyllosilicates on the surface of Ceres
E. Ammannito, M. C. DeSanctis, M. Ciarniello, A. Frigeri, F. G. Carrozzo, J.-Ph. Combe, B. L. Ehlmann, S. Marchi, H. Y. McSween, A. Raponi, M. J. Toplis, F. Tosi, J. C. Castillo-Rogez, F. Capaccioni, M. T. Capria, S. Fonte, M. Giardino, R. Jaumann, A. Longobardo, S. P. Joy, G. Magni, T. B. McCord, L. A. McFadden, E. Palomba, C. M. Pieters, C. A. Polanskey, M. D. Rayman, C. A. Raymond, P. M. Schenk, F. Zambon and C. T. Russell (September 1, 2016)
Science **353** (6303), . [doi: 10.1126/science.aaf4279]

Editor's Summary

Science (print ISSN 0036-8075; online ISSN 1095-9203) is published weekly, except the last week in December, by the American Association for the Advancement of Science, 1200 New York Avenue NW, Washington, DC 20005.